

MOX-Report No. 70/2022

Mathematical modelling of axonal cortex contractility

Andrini, D.; Balbi, V.; Bevilacqua, G.; Lucci, G.; Pozzi, G.;
Riccobelli, D.

MOX, Dipartimento di Matematica
Politecnico di Milano, Via Bonardi 9 - 20133 Milano (Italy)

mox-dmat@polimi.it

<http://mox.polimi.it>

MATHEMATICAL MODELLING OF AXONAL CORTEX CONTRACTILITY

D. ANDRINI¹, V. BALBI², G. BEVILACQUA³, G. LUCCI³, G. POZZI⁴, AND D. RICCOBELLI⁴

ABSTRACT. The axonal cortex is composed of a regular structure of F-actin and spectrin able to contract thanks to myosin II motors. Such an active tension is of fundamental importance in controlling the physiological shape of axons. Recent experiments show that axons modulate the contraction of the cortex when subject to mechanical deformations, exhibiting a non-trivial coupling between the hoop and the axial active tension. However, the underlying mechanisms are still poorly understood. In this paper, we propose a continuum model of the axon based on the active strain theory. By using the Coleman-Noll procedure, we shed light on the coupling between the hoop and the axial active strain through the Mandel stress tensor. We propose a qualitative analysis of the system under the simplifying assumption of incompressibility, showing the existence of a stable equilibrium solution. In particular, our results show that the axon regulates the active contraction to maintain a homeostatic stress state. Finally, we propose numerical simulations of the model, using a more suitable compressible constitutive law. The results are compared with experimental data, showing an excellent quantitative agreement.

STATEMENT OF SIGNIFICANCE. The mechanics of cortical contractility in axons is still poorly understood. Unraveling the mechanisms underlying axial and hoop stress generation in the cortex will give insight on the active regulation of axon diameter. The understanding of this phenomenon may shed new light on the physical causes of axonal morphological degeneration as a consequence of neurodegenerative diseases, viral infections, and traumatic brain injuries.

1. INTRODUCTION

Axons are fundamental structures of neurons whose purpose is the transmission of electrochemical signals to neighbouring cells. The inner part, called *axoplasm*, is the cytoplasm of axons and contains several organelles and microtubules. The latter are cross-linked together forming a network which gives the axoplasm an elastic behaviour. The axoplasm is surrounded by a coating, called *cortex*, composed of F-actin, namely polymer microfilaments made of actin, interconnected together by myosin II molecular motors and spectrin. In particular, the actin cortex can actively contract thanks to the action of myosin II. The interplay between the microtubule network and the cortical actomyosin machinery aims at maintaining the cylindrical shape of the axon [33].

Many phenomena can alter such a delicate dynamic equilibrium. In particular, the disruption of the elastic component of the axoplasm during stretch can lead to bulging along the axon, a process called axonal *beading* or *pearling*, a hallmark of neuronal damage [26, 13]. Indeed, axons can sustain large deformations, up to 100%, if the strain is slowly and progressively imposed [43]. Under such conditions, the elastic deformation can even induce an axial growth of the axon thanks to the production of new microtubules [47, 9, 8, 32]. Conversely, rapid stretching of the axon can lead to a damage of the cytoskeleton and to the depolymerisation of microtubules [43, 6].

Axonal beading has been observed as a consequence of several pathological conditions, such as the Alzheimer's [40] and Parkinson's diseases [42], viral infections [24], and multiple sclerosis [31]. There is increasing evidence that all these conditions result in structural damage of the cytoskeleton. Indeed, it has been shown that axonal beading can be explained by a mechanical instability triggered by both the reduction of axoplasm stiffness and the active contraction of

(1) SISSA – INTERNATIONAL SCHOOL FOR ADVANCED STUDIES, VIA BONOMEA 265, 34136, TRIESTE, ITALY

(2) SCHOOL OF MATHEMATICAL AND STATISTICAL SCIENCES, UNIVERSITY OF GALWAY, UNIVERSITY ROAD, H91 TK33, GALWAY, IRELAND

(3) DEPARTMENT OF MATHEMATICAL SCIENCES, POLITECNICO DI TORINO, CORSO DUCA DEGLI ABRUZZI 24, 10129, TORINO, ITALY

(4) MOX – DIPARTIMENTO DI MATEMATICA, POLITECNICO DI MILANO, PIAZZA LEONARDO DA VINCI 32, 20133, MILANO, ITALY

E-mail addresses: dandrini@sissa.it, vbalbi@nuigalway.ie, giulia.bevilacqua@polito.it, giulio.lucci@polito.it, giulia.pozzi@polimi.it, davide.riccobelli@polimi.it.

the actin cortex [36]. Therefore, unveiling the mechanism underlying cortical contraction is of utmost importance to understand how axons maintain their structural stability and to prevent their degeneration.

Experimental observations show that actin filaments are arranged in a geometrically regular pattern, forming circles spaced at a constant distance of 180 nm-190 nm along the axonal length, interconnected by spectrin and myosin II [45]. Such a microstructural organisation suggests that the actin cortex can generate an active tension in both the axial and the circumferential direction. Recent experiments have linked hoop contractility to the self-regulation of the axon diameter following an externally imposed axial stretch, microtubule depolymerisation or myosin II disruption [18, 12]. In these works, the authors suggest that such changes may be induced by the compressive force exerted on the axoplasm by the active contraction of the cortex [18]. Furthermore, an active diameter reduction is observed when axons are axially stretched, suggesting a coupling between axial and hoop active tensions. However, the nature of such a coupling is still not understood.

In this paper, we use tools of Continuum Mechanics to investigate the non-trivial coupling between the axial and circumferential active contractions and we show that the cortex contractility induces a compression in the axoplasm. The paper is organised as follows: in Section 2, we propose a continuum model of the axon. By using the active strain approach and the Coleman–Noll procedure, we obtain the evolution equations for the coupled hoop and axial active stretches. In Section 3, we assume the axon to be incompressible and we show that the above mentioned equations reduce to a simple dynamical system that can be easily studied analytically. In Section 4, we assume a more appropriate compressible behaviour and we numerically approximate the mathematical model. We then compare quantitatively our numerical results with experimental results available in the literature. Finally, in Section 5, we discuss the main outcomes of the paper together with some important concluding remarks.

2. MATHEMATICAL MODEL

The aim of this Section is to construct a mathematical model of actin cortex contraction and to investigate the coupling between the axial and the circumferential contractility using the framework of Continuum Mechanics.

2.1. Notation and kinematics. We model the axon as a continuum body with reference configuration

$$\Omega_0 = \{ \mathbf{X} \in \mathbb{E}^3 \mid R \in [0, R_o], \Theta \in [0, 2\pi], Z \in \mathbb{R} \},$$

where R, Θ, Z are the Lagrangian cylindrical coordinates of the material point

$$\mathbf{X} = (R \cos \Theta, R \sin \Theta, Z)$$

belonging to the three dimensional Euclidean space \mathbb{E}^3 , with $(\mathbf{E}_R, \mathbf{E}_\Theta, \mathbf{E}_Z)$ being the corresponding vector basis. Due to the slenderness of the axon we assume the reference domain to be infinite along \mathbf{E}_Z .

The axon is composed of an inner part Ω_{0a} and an outer coating Ω_{0c} , representing the axoplasm and the actin cortex, respectively. More explicitly, we define

$$\begin{aligned} \Omega_{0a} &= \{ \mathbf{X} \in \Omega_0 \mid 0 \leq R < R_i \}, \\ \Omega_{0c} &= \{ \mathbf{X} \in \Omega_0 \mid R_i \leq R \leq R_o \}, \end{aligned}$$

where R_i is the internal radius of the axoplasm.

Let $\varphi : [t_0, t_1] \times \Omega_0 \rightarrow \mathbb{E}^3$ be the motion of Ω_0 , so that $\mathbf{x} = \varphi(t, \mathbf{X})$ is the actual position vector of point \mathbf{X} at time t . We denote by r, θ, z the coordinate of \mathbf{x} in a cylindrical reference frame where $(\mathbf{e}_r, \mathbf{e}_\theta, \mathbf{e}_z)$ is the corresponding vector basis.

Let $\mathbf{F} = \text{Grad } \varphi$ be the deformation gradient. To model the active contraction of the cortex, we use the active strain approach [5, 20]. This method was first developed to model muscle contraction [25, 41, 30, 37] and has been recently used to model axonal contractility [19, 36]. We then assume a multiplicative decomposition of the deformation gradient as follows

$$\mathbf{F} = \mathbf{F}_e \mathbf{F}_a,$$

where \mathbf{F}_e and \mathbf{F}_a account for the elastic and the inelastic active distortion, respectively. The tensor \mathbf{F}_a describes the contractility of the cortex and has to be constitutively prescribed (see Figure 1).

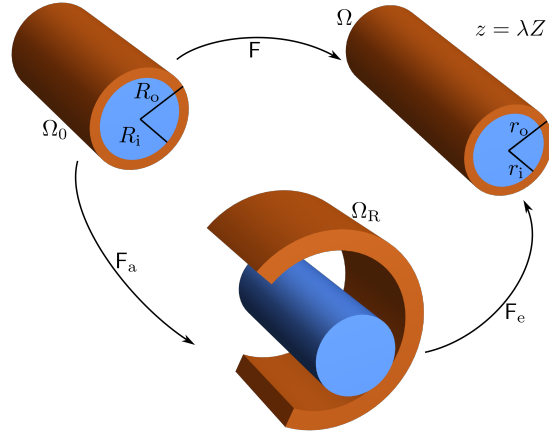


FIGURE 1. Representation of the multiplicative decomposition of the deformation gradient $\mathbf{F} = \mathbf{F}_e \mathbf{F}_a$.

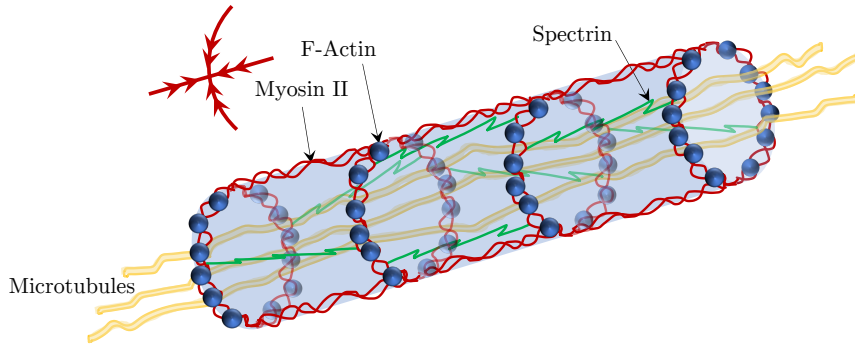


FIGURE 2. Micro-structure of the axon: in the cortex, the actin filaments are arranged in rings around the circumference of the axon. The myosin II motors both connect the actin rings and run along the length of the axon, creating a coupled contraction in the circumferential and the longitudinal directions.

We also denote by J , J_e , and J_a the determinants of the tensors \mathbf{F} , \mathbf{F}_e , and \mathbf{F}_a , respectively, representing the local change of volume induced by the relative distortion field.

As shown in Figure 2, the cortex of the axon has a highly organised structure whereby the F-actin rings, arranged along the circumference of the axon, are connected by the myosin II motors [12]. The myosin motors also run along the longitudinal direction and generate an axial contraction. Spectrin filaments contribute to the structural integrity and the elasticity of axons. Given this specific micro-structural organisation of the cortex, we can reasonably assume that

$$(1) \quad \mathbf{F}_a = \frac{1}{a_\Theta a_Z} \mathbf{E}_R \otimes \mathbf{E}_R + a_\Theta \mathbf{E}_\Theta \otimes \mathbf{E}_\Theta + a_Z \mathbf{E}_Z \otimes \mathbf{E}_Z,$$

for $\mathbf{X} \in \Omega_{0c}$, where a_Θ and a_Z are the active stretches along the circumferential and the axial direction, respectively. In this way, the active strain tensor accounts for a pure remodelling of the cortex [17], i.e. $J_a = 1$, without any volume modification (contrary to growth/resorption).

As already discussed, the active contraction is localised in the cortex. Hence, we model the axoplasm as a passive elastic material by setting $\mathbf{F}_a = \mathbf{I}$. As for the cortex, we assume that the reference configuration Ω_{0c} corresponds to a relaxed condition in which all the active fibers are fully extended. Hence, a further reciprocal sliding of the actin and myosin filaments cannot take place without generating mechanical stress. Mathematically, this conditions translates into a unilateral constraint which forces the active stretches to be less than one, namely, $a_\Theta, a_Z \leq 1$.

2.2. Balance equations and boundary conditions. In this Section, we specify the balance laws of the model. First, we enforce the balance of the linear momentum. In the absence of external body forces and by neglecting inertia, the balance of linear momentum reduces to the following equation

$$(2) \quad \text{Div } \mathbf{P} = \mathbf{0},$$

where \mathbf{P} is the first Piola-Kirchhoff stress tensor and Div represents the divergence in material coordinates. Equivalently, the balance of the linear momentum can be recast in the actual configuration as follows

$$(3) \quad \text{div } \mathbf{T} = \mathbf{0},$$

where \mathbf{T} is the Cauchy stress tensor and div is the divergence operator in the actual reference frame. The Cauchy stress is related to \mathbf{P} through the relation

$$(4) \quad \mathbf{T} = J^{-1} \mathbf{P} \mathbf{F}^T$$

For later convenience, we also introduce the Mandel stress tensor, defined as

$$(5) \quad \mathbf{M} = \mathbf{F}_e^T \mathbf{P} \mathbf{F}_a^T = J \mathbf{F}_e^T \mathbf{T} \mathbf{F}_e^{-T},$$

which is another measure of the stress commonly used in the theory of plasticity [29, 22].

The balance equations are complemented by proper boundary and interface conditions. We assume that the external boundary of the axon is free of traction, therefore

$$(6) \quad \mathbf{P} \mathbf{N} = \mathbf{0} \quad \text{where } R = R_o,$$

where \mathbf{N} is the outward normal in the initial configuration. We also enforce the continuity of displacement and traction at the interface between the cortex and the axoplasm, namely

$$(7) \quad \begin{cases} \lim_{R \rightarrow R_i^-} \mathbf{u} = \lim_{R \rightarrow R_i^+} \mathbf{u}, \\ \lim_{R \rightarrow R_i^-} \mathbf{P} \mathbf{N} = \lim_{R \rightarrow R_i^+} \mathbf{P} \mathbf{N}. \end{cases}$$

Since the actin cortex is made of an active material, we must describe the active process underlying its contraction by introducing additional balance equations. Specifically, the active strain tensor (1) introduces two additional kinematic variables: a_Θ and a_Z . Changes in a_Θ and a_Z describe the microstructural reorganisation of the actin cortex. In particular, the cortex can undergo remodelling as a result of external stimuli, such as the presence of ATP molecules. By following the theory developed in [16], we model such external stimuli by introducing two scalar fields, B_Θ and B_Z . These fields play the role of external forces that drive cortical contractility in the hoop and in the axial direction, respectively. We label B_Θ and B_Z as external remodelling (or active) stresses.

Such external remodelling stresses induce an inelastic distortion of the material, i.e. the actin filaments undergo a microstructural reorganisation. The response of the material to the external stimuli (e.g. how much and how fast the actin filaments contracts in the presence of a given concentration of ATP) depends on how the cortex is organized. This material property is modeled by the scalars C_Θ and C_Z , representing the resistance of the cortex to the contraction in the hoop and in the axial direction. On the one hand, B_Θ and B_Z represent the action of external entities. On the other hand, C_Θ and C_Z are called internal remodelling (or active) stresses.

By following [16], we prescribe a balance between the remodelling stresses that drive the cortex contractility as follows

$$(8) \quad \begin{cases} B_\Theta = C_\Theta, \\ B_Z = C_Z. \end{cases}$$

In the next section, we provide the constitutive equations for the materials and the evolution laws for the active stretches.

2.3. Thermodynamics restrictions and Coleman-Noll procedure. In the following, we use the so-called Coleman-Noll [11] procedure, which is based on the Clausius-Duhem inequality, and we derive the constitutive and evolution laws. Specifically, we postulate the existence of a strain energy density function Ψ and, following [16], we write the Clausius-Duhem inequality

$$(9) \quad \int_{\mathcal{P}} \dot{\Psi} \, dV \leq \int_{\mathcal{P}} \mathbf{P} : \dot{\mathbf{F}} \, dV + \int_{\mathcal{P} \cap \Omega_{0c}} \left[C_{\Theta} \frac{\dot{a}_{\Theta}}{a_{\Theta}} + C_Z \frac{\dot{a}_Z}{a_Z} \right] \, dV,$$

where \mathcal{P} is a subdomain of Ω_0 . The superposed dot denotes the time derivative, and $\mathbf{A} : \mathbf{B} = \text{tr}(\mathbf{A}^T \mathbf{B})$. We remark that the last integral in (9) represents the power of the internal remodelling forces and is performed on $\mathcal{P} \cap \Omega_{0c}$, since only the cortex can actively contract.

By following the principle of equipresence [44], we postulate that the constitutive relations for Ψ , C_{Θ} , C_Z , and \mathbf{P} depend on the same kinematic quantities. Here, we assume that

$$\Psi = \Psi(\mathbf{X}, \mathbf{F}, a_j, \dot{a}_j), \quad C_j = C_j(\mathbf{X}, \mathbf{F}, a_j, \dot{a}_j), \quad \mathbf{P} = \mathbf{P}(\mathbf{X}, \mathbf{F}, a_j, \dot{a}_j),$$

where $j = \Theta, Z$.

Under such assumptions, we can rewrite (9) as follows

$$(10) \quad \int_{\mathcal{P}} \left(\frac{\partial \Psi}{\partial \mathbf{F}} - \mathbf{P} \right) : \dot{\mathbf{F}} \, dV + \int_{\mathcal{P} \cap \Omega_{0c}} \sum_{j=\Theta, Z} \left(\frac{\partial \Psi}{\partial a_j} a_j - C_j \right) \frac{\dot{a}_j}{a_j} \, dV + \int_{\mathcal{P} \cap \Omega_{0c}} \frac{\partial \Psi}{\partial \dot{a}_j} \ddot{a}_j \, dV \leq 0,$$

which must hold for any admissible process [11, 34]. Thus, from the arbitrariness of $\dot{\mathbf{F}}$ and \ddot{a}_j , we obtain

$$(11) \quad \mathbf{P} = \frac{\partial \Psi}{\partial \mathbf{F}}, \quad \frac{\partial \Psi}{\partial \dot{a}_j} = 0,$$

where the first relation is the classic expression of the first Piola-Kirchhoff stress tensor of a hyperelastic material, while the second one states that the energy Ψ is independent of \dot{a}_{Θ} and \dot{a}_Z .

By considering every admissible \dot{a}_j , $j = \Theta, Z$, we can further enforce the Clausius-Duhem inequality (10). We then find that a constitutive law for C_{Θ} and C_Z satisfying (10) is given by¹

$$(12) \quad C_j = \frac{\partial \Psi}{\partial a_j} a_j + \mu_c \tau_j \frac{\dot{a}_j}{a_j} + \Gamma_j,$$

where μ_c is the shear modulus of the cortex and τ_j is the characteristic time of axonal contractility. The additional variable Γ_j is the reactive term which enforces the unilateral constraint $a_j \leq 1$ and plays the role of a Lagrange multiplier. Γ_j can be physically interpreted as the force which prevents the actin and myosin filaments from sliding on each other beyond a certain threshold. More specifically, Γ_j satisfies the following relations

$$(13) \quad \begin{cases} \Gamma_j(a_j - 1) = 0, \\ \Gamma_j \geq 0. \end{cases}$$

We observe that Γ_j is zero whenever $a_j \neq 1$. By using (8) and (12), we get

$$(14) \quad \dot{a}_j = \frac{a_j}{\mu_c \tau_j} \left(B_j - \frac{\partial \Psi}{\partial a_j} a_j - \Gamma_j \right).$$

If $a_j = 1$, i.e. we are on the boundary of the unilateral constraint $a_j \leq 1$, and $\dot{a}_j|_{t=t_0} = 0$, from (14) we get

$$\Gamma_j = B_j - \frac{\partial \Psi}{\partial a_j} a_j,$$

which holds whenever $\Gamma_j \geq 0$, namely when $B_j \geq a_j \partial \Psi / \partial a_j$. Conversely, if $B_j < a_j \partial \Psi / \partial a_j$, from (14) we observe that $\dot{a}_j|_{t=t_0}$ is negative, therefore $a_j(t) < 1$ in a right neighborhood of t_0 . In summary, when $a_j = 1$ the reactive term Γ_j is given by

$$(15) \quad \Gamma_j = \max \left\{ 0, B_j - \frac{\partial \Psi}{\partial a_j} a_j \right\}.$$

¹We stress that the restrictions on C_{Θ} and C_Z depend on the power of the remodelling forces postulated in (9). For an extensive discussion see [21], §14. In addition we remark that the dissipative term in (12) is just one of the admissible choices compatible with the Clausius-Duhem inequality, see [4].

By following the active strain approach [25, 41], we now use the multiplicative decomposition of the deformation gradient. Let Ψ_0 be the strain energy density of the passive material, we define the active free energy density as

$$(16) \quad \Psi(\mathbf{X}, \mathbf{F}, a_\Theta, a_Z) = \Psi_0(\mathbf{X}, \mathbf{F}\mathbf{F}_a^{-1}).$$

With the newly defined energy density in the equation above, from (11) we get

$$(17) \quad \mathbf{P} = \frac{\partial \Psi_0}{\partial \mathbf{F}_e} \mathbf{F}_a^{-T}.$$

By using (16), we obtain

$$(18) \quad \frac{\partial \Psi}{\partial a_j} = -\mathbf{M} : \left(\frac{\partial \mathbf{F}_a}{\partial a_j} \mathbf{F}_a^{-1} \right), \quad \text{with } \mathbf{M} = \mathbf{F}_e^T \frac{\partial \Psi_0}{\partial \mathbf{F}_e},$$

where \mathbf{M} is the Mandel stress tensor defined in (5). By introducing the tensors

$$\mathbf{l}_\Theta = \mathbf{E}_\Theta \otimes \mathbf{E}_\Theta - \mathbf{E}_R \otimes \mathbf{E}_R, \quad \mathbf{l}_Z = \mathbf{E}_Z \otimes \mathbf{E}_Z - \mathbf{E}_R \otimes \mathbf{E}_R,$$

and by combining (1) with (18), we get

$$(19) \quad \frac{\partial \Psi}{\partial a_j} a_j = -\mathbf{M} : \mathbf{l}_j.$$

Thus, by substituting (19) into (14) and by enforcing (15), we finally get

$$(20) \quad \dot{a}_j = \begin{cases} \frac{a_j}{\mu_c \tau_j} (B_j + \mathbf{M} : \mathbf{l}_j), & \text{if } a_j < 1 \text{ or } B_j < -\mathbf{M} : \mathbf{l}_j, \\ 0, & \text{otherwise,} \end{cases}$$

where again $j = \Theta, Z$.

The evolution equations (20) for a_Θ and a_Z can be used to provide a physical interpretation of the external remodelling stress in (8). Similarly to the growth processes studied in [16, 4], B_Θ and B_Z represent the external forces that drive the active contraction of the cortex. Moreover, we observe that when the linear combinations of the Mandel stress components $\mathbf{M} : \mathbf{l}_\Theta$ and $\mathbf{M} : \mathbf{l}_Z$ are equal to $-B_\Theta$ and $-B_Z$, respectively, the system is in chemo-mechanical equilibrium. Therefore, B_Θ and B_Z can be regarded as the equilibrium, or *homeostatic*, stresses towards which the system is led.

Despite sharing many similarities with the growth models developed in [4], our approach has the following unique features. First, the active strain tensor is isochoric, namely $J_a = 1$. The effect of such a restriction is that the Mandel stress appears in (20) in place of the Eshelby stress (see for instance equations (2.24) and (3.2) in [4]). Secondly, \mathbf{F}_a is not a generic tensor with positive determinant but belongs to the subset described by (1). Thus, only a particular combination of the Mandel stress components are involved in the evolution equations (20).

A similar approach has been recently adopted by Deghany et al. in [14] to model F-actin contractility in axons. In their work, the authors used an approach inspired by smooth muscles models, such as those developed by Stålhand et al. in [39]. Our model considers a more general form for the active strain tensor. Instead of being prescribed *a priori*, the active strains a_Θ and a_Z are initially decoupled and their coupling is later provided by the Coleman-Noll procedure, through the Mandel stress tensor. In particular, the assumption of a linear relationship between a_Θ and a_Z such as $a_Z = \beta a_\Theta$ can lead to some issues (for instance, the tensor \mathbf{F}_a cannot be equal to the identity when $\beta \neq 1$). The *a priori* assumption $a_\Theta = a_Z$ is thoroughly analyzed in the following and we refer to it as the *monoparametric approach*. Furthermore, the theoretical framework presented in this Section is based on the balance equations proposed by DiCarlo and Quiligotti in [16] and allows us to clarify the key role of the Mandel tensor in regulating the stress distribution within the axon.

2.4. Symmetry assumptions. Experimental evidence [18] suggests that changes in axonal external radius are invariant along \mathbf{E}_Z . We therefore assume the axon deformation to be axisymmetric by enforcing the following simplified kinematics

$$(21) \quad \boldsymbol{\varphi}(t, \mathbf{X}) = r(t, R)\mathbf{e}_r + \lambda Z\mathbf{e}_z,$$

with $\lambda \in (0, +\infty)$ being the imposed axial stretch along Z . Thus, the deformation gradient reads

$$(22) \quad \mathbf{F} = \frac{\partial r}{\partial R} \mathbf{e}_r \otimes \mathbf{E}_R + \frac{r}{R} \mathbf{e}_\theta \otimes \mathbf{E}_\Theta + \lambda \mathbf{e}_z \otimes \mathbf{E}_Z,$$

where $r(t, R) = R + u(t, R)$ with u representing the radial displacement. Under the assumption (21), the balance of linear momentum (2) takes the following form

$$(23) \quad \frac{dP_{RR}}{dR} + \frac{P_{RR} - P_{\Theta\Theta}}{R} = 0,$$

where P_{RR} and $P_{\Theta\Theta}$ are the radial and the hoop components of the first Piola-Kirchhoff stress tensor, respectively. In terms of the Cauchy stress tensor the balance reads as follows

$$(24) \quad \frac{dT_{rr}}{dr} + \frac{T_{rr} - T_{\theta\theta}}{r} = 0,$$

where T_{rr} and $T_{\theta\theta}$ are the radial and hoop components of \mathbb{T} . The balance of linear momentum must be solved with respect to the radial displacement u , either in material or spatial coordinates. Moreover, u must satisfy the homogeneous Dirichlet boundary conditions $u(t, 0) = 0$ to ensure the continuity of the deformation field along the Z axis. By enforcing (21), the boundary condition (6) reduces to the scalar equation

$$(25) \quad P_{RR}|_{R=R_o} = 0,$$

or, equivalently, in the actual configuration

$$(26) \quad T_{rr}|_{r=r_o} = 0,$$

where $r_o = r(t, R_o)$. Equation (23) endowed with the above mentioned boundary condition should be coupled with (20) to completely describe the axon dynamics.

3. QUALITATIVE ANALYSIS: THE INCOMPRESSIBLE CASE

In the following, we analyse the evolution equations (20) for the particular case where the axon is treated as an incompressible medium. Such a simplified assumption allows us to provide analytical predictions on the existence and stability of the equilibrium solutions of (20).

To impose the incompressibility constraint, we require that

$$J_e = \det \mathbf{F}_e = 1$$

which, combined with the expression of the active strain tensor (1), implies that $J = \det \mathbf{F} = 1$ as well. The enforcement of the incompressibility constraint can be done by introducing a Lagrange multiplier p . More explicitly, we can introduce the extended strain energy density

$$(27) \quad \Psi_{\text{ext}}(\mathbf{X}, \mathbf{F}, a_\Theta, a_Z, p) = \Psi(\mathbf{X}, \mathbf{F}, a_\Theta, a_Z) - p(J - 1),$$

and then proceed as in the previous section, by replacing Ψ by Ψ_{ext} (see [17] for details). In particular, the Piola-Kirchhoff stress reads as follows

$$\mathbf{P} = \frac{\partial \Psi_0}{\partial \mathbf{F}_e} \mathbf{F}_a^{-T} - p \mathbf{F}^{-T}.$$

The Cauchy and the Mandel stress tensors can be computed by using (4) and (5) to obtain the following constitutive equations

$$\mathbb{T} = \frac{\partial \Psi_0}{\partial \mathbf{F}_e} \mathbf{F}_e^T - pl, \quad \mathbb{M} = \mathbf{F}_e^T \frac{\partial \Psi_0}{\partial \mathbf{F}_e} - pl.$$

As a constitutive choice, we assume that both the cortex and the axoplasm are made of incompressible neo-Hookean materials, i.e.

$$(28) \quad \Psi_0(\mathbf{F}_e) = \frac{\mu}{2} (\mathbf{F}_e : \mathbf{F}_e - 3), \quad \mu = \begin{cases} \mu_a, & R < R_i, \\ \mu_c, & R \geq R_i, \end{cases}$$

where μ_a and μ_c represent the shear moduli of the axoplasm and of the cortex, respectively, and are both positive constants. By using the constitutive assumption (28), we get the following expression for the Cauchy and the Mandel stress tensors

$$(29) \quad \mathbb{T} = \mu \mathbf{F}_e \mathbf{F}_e^T - pl, \quad \mathbb{M} = \mu \mathbf{F}_e^T \mathbf{F}_e - pl.$$

We look for a radially symmetric solution in the form of (21) and we use the incompressibility constraint $J = 1$ to get the following relation

$$r(t, R) = R/\sqrt{\lambda},$$

so that (22) becomes

$$(30) \quad \mathbf{F} = \frac{1}{\sqrt{\lambda}} (\mathbf{e}_r \otimes \mathbf{E}_R + \mathbf{e}_\theta \otimes \mathbf{E}_\Theta) + \lambda \mathbf{e}_z \otimes \mathbf{E}_Z.$$

By using the balance of linear momentum (24), we get

$$(31) \quad p(r) = k_1, \quad 0 \leq r < r_i,$$

$$(32) \quad p(r) = k_2 + \frac{(a_\Theta^4 a_Z^2 - 1) \mu_c \log(r)}{a_\Theta^2 \lambda}, \quad r_i \leq r < r_o,$$

where $r_i = r(t, R_i)$, while k_1 and k_2 are constants and can be determined by using the interface and the boundary conditions (7) and (26), as follows

$$(33) \quad k_1 = \frac{\mu_a}{\lambda} + \frac{\mu_c [\log(r_i) - \log(r_o)] (a_\Theta^4 a_Z^2 - 1)}{a_\Theta^2 \lambda},$$

$$(34) \quad k_2 = \frac{\mu_c [a_Z^2 a_\Theta^4 + \log(r_o) - a_Z^2 a_\Theta^4 \log(r_o)]}{a_\Theta^2 \lambda}.$$

The radial component of the Cauchy stress T_{rr} evaluated at the interface $r = r_i$ can be computed by combining (29)-(34) as follows

$$(35) \quad T_{rr}(r_i) = -\frac{\mu_c (a_\Theta^4 a_Z^2 - 1) [\log(r_i) - \log(r_o)]}{\lambda a_\Theta^2}.$$

Thus, by using the expression of the Mandel stress tensor (29) and (30), the evolution equations (20) reduce to the following dynamical system

$$(36) \quad \begin{cases} \dot{a}_\Theta = \frac{a_\Theta}{\mu_c \tau_\Theta} \left(B_\Theta + \frac{\mu_c (1 - a_\Theta^4 a_Z^2)}{\lambda a_\Theta^2} \right), \\ \dot{a}_Z = \frac{a_Z}{\mu_c \tau_Z} \left(B_Z + \frac{\mu_c (\lambda^3 - a_\Theta^2 a_Z^4)}{\lambda a_Z^2} \right), \end{cases}$$

where the first equation holds whenever $a_\Theta < 1$ or the right-hand side is negative, otherwise $\dot{a}_\Theta = 0$. Similarly, the second equation holds if either $a_Z < 1$ or the corresponding right-hand side is negative, otherwise $\dot{a}_Z = 0$.

3.1. Stability of the equilibria. Throughout the rest of the paper, we will focus on the case where $B_\Theta = B_Z = B < 0$ is spatially constant, so that the external remodelling stresses are homogeneous and share the same value. As we will show in the following, we require B to be negative so that the cortex actively contracts. Moreover, since we are interested in uniaxial stretching of the axon, we focus on the range $\lambda \geq 1$.

By setting $\dot{a}_\Theta = \dot{a}_Z = 0$, we look for equilibrium solutions of (36). By subtracting the two equations, we get

$$(37) \quad a_\Theta^2 = \frac{a_Z^2}{\lambda^3}.$$

We can then substitute (37) into the second of equation (36) which gives the following condition to find the equilibria of the system

$$(38) \quad f(a_Z) = \mu_c a_Z^6 - B \lambda^4 a_Z^2 - \mu_c \lambda^6 = 0.$$

We recall that $B < 0$ and $\lambda \geq 1$, therefore the function f in (38) is strictly increasing and takes values of opposite sign at the endpoints of the interval $[0, 1]$ whenever

$$(39) \quad \frac{B}{\mu_c} < \frac{1 - \lambda^6}{\lambda^4}.$$

Hence, if such condition is satisfied, then the system has a unique equilibrium solution $(\bar{a}_\Theta, \bar{a}_Z)$. In particular, \bar{a}_Z is obtained from (38) and $\bar{a}_\Theta = \bar{a}_Z / \lambda^{3/2}$ is given by (37).

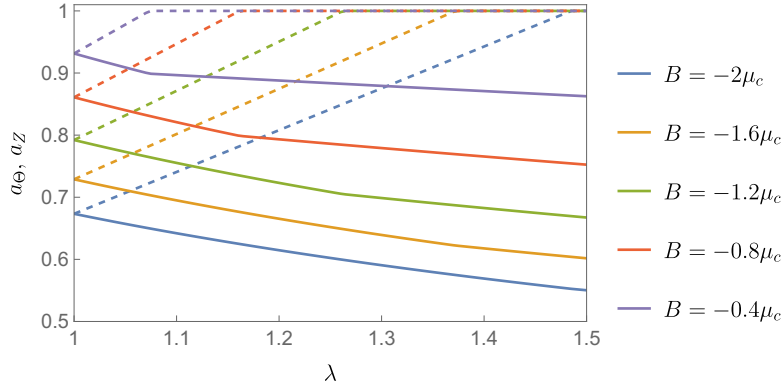


FIGURE 3. Homeostatic active stretches \bar{a}_Θ (solid lines) and \bar{a}_Z (dashed lines) plotted against the applied stretch λ . The curves are obtained from (37), (38), and (42) for $B/\mu_c = -2, -1.6, -1.2, -0.8, -0.4$.

To evaluate the stability of the equilibrium solutions, we compute the Jacobian matrix of the system (36) as follows

$$(40) \quad J = \begin{pmatrix} \frac{a_\Theta^2 \lambda B - \mu_c (1 - 3a_Z^2 a_\Theta^4)}{\lambda \mu_c} \tau_\Theta a_\Theta^2 & -\frac{2a_Z a_\Theta^3}{\lambda \tau_\Theta} \\ -\frac{2a_Z^3 a_\Theta}{\lambda \tau_Z} & \frac{a_Z^2 \lambda B - \mu_c (\lambda^3 - 3a_Z^4 a_\Theta^2)}{\lambda \mu_c \tau_Z a_Z^2} \end{pmatrix}.$$

A direct computation shows that, for all the admissible values of a_Θ and a_Z , we have $\text{tr } J < 0$ and $\det J > 0$. Then, the equilibrium solution $(\bar{a}_\Theta, \bar{a}_Z)$ is asymptotically stable.

On the other hand, if (39) does not hold, i.e.

$$(41) \quad \frac{B}{\mu_c} \geq \frac{1 - \lambda^6}{\lambda^4},$$

we set $\bar{a}_Z = 1$, so that the first equation of (20) admits the equilibrium solution

$$(42) \quad \bar{a}_\Theta = \frac{1}{\sqrt{2}} \sqrt{\sqrt{\frac{B^2}{\mu_c^2} \lambda^2 + 4} + \frac{B\lambda}{\mu_c}},$$

which always lies in $(0, 1)$. Finally we need to check that $B_Z + M : I_Z \geq 0$, so that $\bar{a}_Z = 1$ is a stationary solution of (20). It can be easily verified that such a condition is equivalent to (41). Moreover, such an equilibrium is always stable since the component J_{11} of the Jacobian matrix (40) is negative.

The existence of asymptotically stable equilibria of (20) implies that, depending on the initial conditions, the system evolves towards the equilibrium points \bar{a}_Θ and \bar{a}_Z . These equilibrium values represent the homeostatic active stretches of the axon.

In Figure 3, we plot the stationary solutions \bar{a}_Θ and \bar{a}_Z against the applied stretch λ , for different values of B . Starting from the same value for $\lambda = 1$, the two active stretches \bar{a}_Θ and \bar{a}_Z exhibit opposite behaviours as λ increases. On the one hand, \bar{a}_Θ decreases with λ , leading to a stronger contraction in the circumferential direction which is generated by the actin molecular motors. On the other hand, a_Z increases until it reaches 1.

We remark that, when $\bar{a}_Z < 1$, the radial component of the Cauchy stress at the interface $r = r_i$ (in equation (35)), evaluated at the equilibrium, can be written as follows

$$(43) \quad \bar{T}_{rr}(r_i) = B_\Theta \log \left(\frac{R_o}{R_i} \right),$$

which is independent from the applied stretch λ . Thus, as the axon is axially stretched, the cortex undergoes remodelling to maintain a constant compression in the axoplasm.

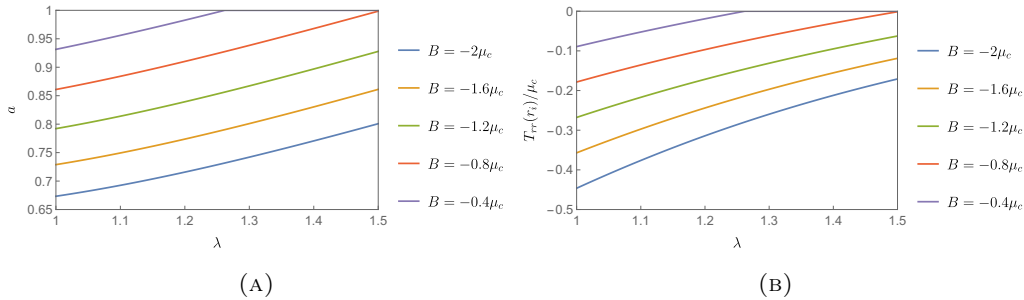


FIGURE 4. Monoparametric approach. (a) Homeostatic active stretch a versus the applied stretch λ . The value of a is computed by using (54). (b) Radial stress at the interface calculated from (45) for $R_i/R_o = 0.8$. In both cases, the curves are obtained with $B/\mu_c = -2, -1.6, -1.2, -0.8, -0.4$.

3.2. Monoparametric active stretch. In [14], the authors directly prescribe a coupling between a_Θ and a_Z , by assuming a linear relation between the two active stretches. In our case, by enforcing $a_\Theta = a_Z = a$ we get

$$(44) \quad \mathbf{F}_a = \frac{1}{a^2} \mathbf{E}_R \otimes \mathbf{E}_R + a(\mathbf{I} - \mathbf{E}_R \otimes \mathbf{E}_R).$$

The corresponding evolution equation for the active stretch a can be obtained by repeating the procedure exposed in Section 2. Similarly to the stability analysis performed in this Section, we find a single asymptotically stable equilibrium, as detailed in A. At the equilibrium, the radial stress at the interface is instead given by

$$(45) \quad \bar{T}_{rr}(r_i) = \frac{\mu_c(\bar{a}^6 - 1)}{\lambda \bar{a}^2} \log\left(\frac{R_o}{R_i}\right).$$

As shown in Fig. 4a, we observe that a is an increasing function of the axial stretch λ . Eventually, for large enough values of λ , the axon behaves as a passive material when a reaches 1. Differently, our approach predicts an opposite behaviour for the hoop active stretch, as reported in Figure 3. Such differences have important consequences on the stress distribution within the axon. While in our model the compression of the axoplasm is independent of λ , as shown in equation (43), in the monoparametric approach the radial stress at the interface relaxes as we increase λ and, eventually, becomes zero, see Figure 4b. This behaviour is the main drawback of such approach since, as we will show in the next Section, axons actively decrease their radius upon stretching thanks to axoplasm compression.²

4. ACTIVE REGULATION OF AXON DIAMETER

In this Section, we investigate the role of cortex contractility in actively regulating the axon diameter. We then use experimental data from the literature to validate our numerical model. We use data from [18], where the authors performed experiments on embryonic drosophila axons and measured the variations in the diameter as a consequence of chemo-mechanical manipulations. In particular, different drugs were used to test the mechanical contribution of specific constituents: nocodazole was applied to depolymerise microtubules, while cytochalasin D was used to disrupt F-actin. The effect of these drugs on the axon is depicted in Figure 5. Axons were then rapidly stretched and elongated by 20% from their initial length. To highlight the effect of each drug on the axon diameter, the authors also compared treated axons with control (untreated) axons.

In order to replicate the experimental results, we relax the simplified assumption of incompressibility (see Section 3). To capture the effect of the active contractility on the axon radius, we thus rely on numerical simulations and we obtain approximate solutions of the mathematical model. We then upgrade our model to include the effect of the different drugs on the mechanical response of the axon.

²In the experiments of Fan et al. [18], the axial stretch is applied fast. We remark that if the towing is slow enough, axial stretch induces both an axial and radial growth of the axon [23].

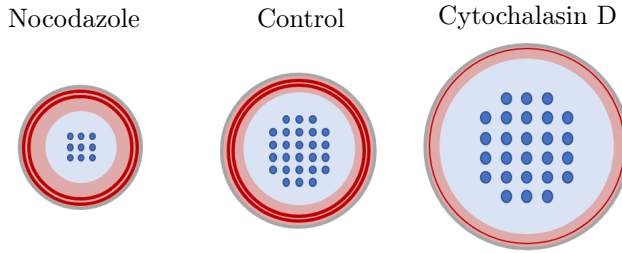


FIGURE 5. Effect of drugs on the axon structure: red lines represent actin filaments while blue circles indicate microtubules. With respect to the control case (center), nocodazole depolymerises microtubules (left) leading to a reduction of the axon diameter, while cytochalasin D reduces the number of the actin filaments (right) and the axon can expand.

4.1. Damage. Experimental evidence shows that the axon stiffness decreases when samples are exposed to nocodazole and cytochalasin D [33]. We model the structural damage of the axon by introducing a scalar field $\alpha : [t_0, t_1] \times \Omega_0 \rightarrow [0, 1]$ that describes the percentage of solid material depolymerised by the action of the drug or during the stretch. The free energy for the damaged axon can then be written as

$$(46) \quad \Psi(\mathbf{F}, \alpha) = (1 - \alpha)\Psi_0(\mathbf{F}\mathbf{F}_a^{-1}),$$

where Ψ_0 is the strain energy density of the passive, sound axon. Initially, the axon is not damaged and therefore

$$\alpha(t = 0, \mathbf{X}) = 0.$$

When nocodazole is applied, the actin cortex is not affected and only the microtubule network is damaged. Therefore, we propose the following simple phenomenological law for the damage of the axoplasm, which describes an exponential degradation

$$(47) \quad \alpha(t, \mathbf{X}) = \begin{cases} \alpha_n^\infty (1 - e^{-t/\tau_n}), & R < R_i, \\ 0, & R > R_i. \end{cases}$$

Here, α_n^∞ is a constant associated to the percentage of microtubules depolymerised in an infinite amount of time, while τ_n is the characteristic time for the action of nocodazole.

Symbol	Parameter description	Range	Value	Reference
R_o	Axon radius	[1.45 μm , 1.90 μm]	1.5 μm	[18]
$R_o - R_i$	Cortex thickness	[0.1 μm , 0.5 μm]	0.3 μm	[27, 19]
μ_c	Cortex shear modulus	[0.1 kPa, 10 kPa]	1 kPa	[15, 7, 19, 46]
μ_a	Axoplasm shear modulus	[0.1 kPa, 10 kPa]	1 kPa	[15, 7, 19, 46]
Λ_c	Cortex I Lamé's coefficient	[0.21 kPa, $+\infty$]	100 kPa	[19, 14, 46]
Λ_a	Axoplasm I Lamé's coefficient	[0, 0.29 kPa]	0.1 kPa	[19, 14]
B_0	External remodelling stress	—	-1.6 kPa	Estimated
τ	Active contraction characteristic time	~ 10 min	11.7 min	[18]
τ_n	Nocodazole characteristic time	[8.5 min, 83.4 min]	20 min	[13]
τ_c	Cytochalasin D characteristic time	~ 10 min	10 min	[38, 18]
α_n^∞	Nocodazole damage	—	0.65	Estimated
α_c^∞	Cytochalasin D damage	—	0.9	Estimated
α_s	Stretch induced damage	—	0.1/0.75	Estimated

TABLE 1. Values of parameters involved in the model. The stretch induced damage has been set equal to 0.75 in the control case and when cytochalasin D is applied. In the case of nocodazole treated axons, the parameter is decreased to 0.1 since the axoplasm is already damaged. With the exception of [19], the cortex is frequently treated as an almost incompressible medium, thus we have chosen a high value for Λ_c .

When cytochalasin D is applied, the contractility of the cortex is reduced and the actin filaments are depolymerised, thus damaging the elastic response of the cortex [38]. Therefore, similarly to nocodazole, we assume that the damage field α follows the law below

$$(48) \quad \alpha(t, \mathbf{X}) = \begin{cases} 0, & R < R_i, \\ \alpha_c^\infty (1 - e^{-t/\tau_c}), & R > R_i, \end{cases}$$

where α_c^∞ and τ_c play the same role as α_n^∞ and τ_n in (47). Furthermore, we postulate that cytochalasin D also reduces the contractility of the actin cortex by modulating the homeostatic stress in (8). For sake of simplicity, we take $B_\Theta = B_Z = B$ and we also assume that the contraction in the circumferential and axial direction share the same characteristic time, i.e. $\tau_\Theta = \tau_Z = \tau$ in (20). Here, we postulate that the reduction of the external remodelling stress due to damage writes as follows

$$B(t, \mathbf{X}) = (1 - \alpha(t, \mathbf{X}))^2 B_0,$$

where B_0 denotes the homeostatic stress in the intact axon.

In [18], Fan and co-authors observed that, when loads are removed, the final radius is smaller than the initial one. The authors concluded that this phenomenon was induced by the damage of the axoplasm. Indeed, a fast axial stretch can induce microtubule depolymerisation [43]. We model this phenomenon by introducing an instantaneous damage in the axoplasm, i.e. we increase $\alpha(t, \mathbf{X})$ by adding a constant α_s for $R < R_i$.

4.2. Constitutive assumptions. For sake of simplicity, we neglect any anisotropy induced by the orientation of microtubules or actin filaments. We assume that both the axoplasm and the cortex are made of a compressible neo-Hookean material. We therefore write the strain energy as follows

$$(49) \quad \Psi_0(\mathbf{F}_e) = \frac{\mu}{2} (\mathbf{F}_e : \mathbf{F}_e - 2 \log J_e - 3) + \frac{\Lambda}{2} (\log J_e)^2,$$

where μ and Λ are the Lamé coefficients of the intact axon. The axoplasm and the cortex are homogeneous, so that the Lamé coefficients are piecewise constant within the domain

$$\mu = \begin{cases} \mu_a, & R < R_i, \\ \mu_c, & R > R_i, \end{cases} \quad \Lambda_0 = \begin{cases} \Lambda_a, & R < R_i, \\ \Lambda_c, & R > R_i. \end{cases}$$

In the next Section, we propose a numerical scheme to discretise the model.

4.3. Initial conditions. In the experiments reported in [18], the axons are in their equilibrium state at the initial instant of time. Thus, we set $\lambda = 1$ and

$$\begin{cases} \alpha|_{t=0} = 0, \\ u|_{t=0} = u_0, \\ a_\Theta|_{t=0} = a_{\Theta 0}, \\ a_Z|_{t=0} = a_{Z 0}, \end{cases}$$

as initial conditions, where u_0 , $a_{\Theta 0}$, and $a_{Z 0}$ are the stationary solutions of (20) and (23). Such equilibrium state has to be determined by means of numerical computations.

4.4. Numerical implementation. Here, we detail the numerical implementation of the problem under the cylindrical symmetry assumptions discussed in Section 2.4. Since the problem is independent of Z , we consider a cylindrical portion of the axon as follows

$$\mathcal{B}_0 = \{\mathbf{X} \in \Omega_0 \mid 0 < Z < 1\}.$$

The strain energy of \mathcal{B}_0 is given by

$$(50) \quad \mathcal{W}(u) = \int_{\mathcal{B}_0} \Psi(\mathbf{F}, \alpha) \, dV = \int_0^{R_0} 2\pi R \Psi(\mathbf{F}, \alpha) \, dR,$$

where we have used the cylindrical symmetry assumed in (21) and Ψ is defined in (46). The function $u : (0, R_0) \rightarrow \mathbb{R}$ satisfies the balance of linear momentum (23) and makes the functional (50) stationary (see [10] for details), i.e.

$$(51) \quad \delta \mathcal{W}(u)[v] = 0 \quad \forall v \in V,$$

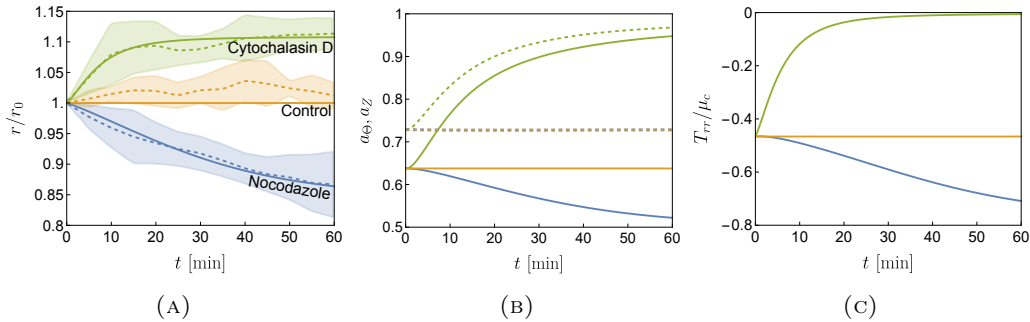


FIGURE 6. Unstretched axons ($\lambda = 1$). Plots are reported for each treatment scenario: control (orange), nocodazole (blue) and cytochalasin (green). (a) Comparison between the numerical result (continuous lines) and the experimental data reported in [18] (dashed lines) for the evolution of external radius. The latter is normalised with respect to r_0 , the radius of the axon at equilibrium. The shaded regions indicate error bar in standard deviation relatively to the experimental data. (b) Plots of a_θ (continuous lines) and a_z (dashed lines) averaged over the cortex sectional area. (c) Evolution of radial stress T_{rr} at the interface $r = r_i$, normalised with respect to the undamaged shear modulus of the cortex.

where v is a real scalar function on the interval $(0, R_o)$. Specifically, the functional space V is defined as

$$V = \{v \in H^1(0, R_o) \mid v(0) = 0\},$$

where $H^1(0, R_o)$ is the space of square-integrable function over $(0, R_o)$ admitting a square-integrable weak derivative. For details see [35].

The spatial computational domain $(0, R_o)$, is subdivided into 500 elements. The time step of the simulations is $\Delta t = 0.3$ minutes. We approximate the radial displacement field u with continuous piece-wise linear functions, while the active stretches a_θ and a_z are discretised by means of piece-wise constant functions.

We solve the equation (51) at each timestep, while the time integration of the evolution equations (20) is performed by using an explicit Euler scheme. The numerical algorithm is implemented using the Python library FEniCS [2, 28]. We use PETSc as linear algebra back-end. In particular, the variational formulation (51) is computed by means of the automatic differentiation tools provided by UFL [3]. Our numerical code can be accessed in [1].

4.5. Results of the simulations. In the following, we present and discuss the results of the numerical simulations. First, we analyse the effect of drugs in unstretched axons (i.e. $\lambda = 1$). Then, in accordance with the experimental procedure proposed in [18], we impose an elongation of the axon up to 20% of its initial length (i.e. $\lambda = 1.2$) and analyse its effect following a one-hour-long exposure to drugs.

We refer to Table 1 for details on the choice of the model parameters.

4.5.1. Effect of drugs on unstretched axons. First, we remark that untreated axons maintain the initial equilibrium state since they are not damaged.

In all the cases, the active contraction of the cortex induces a compressive stress on the axoplasm. The depolymerisation of microtubules due to nocodazole leads to a reduction of the radius and modifies the cortical stress state. Interestingly, the active remodeling forces induce a progressive decrease of a_θ to restore the equilibrium state, as shown in Figure 6b. On the other hand, the axial active stretch a_z does not undergo significant variations. The increase in the circumferential contraction results into a greater compression exerted by the cortex on the axoplasm (i.e. T_{rr} at the interface is negative and decreases, as shown in Figure 6c). In summary, the reduction of the axonal radius following nocodazole exposure is due to the coupling between microtubule depolymerisation and the circumferential active contraction. The longitudinal active stretch instead features an imperceptible deviation from the equilibrium configuration.

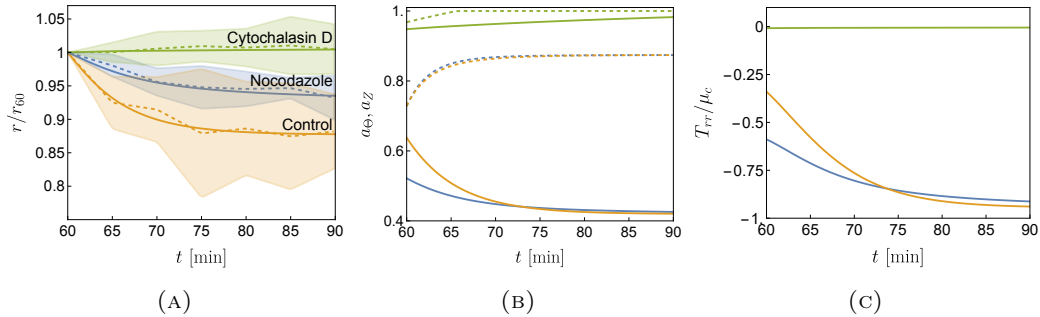


FIGURE 7. Uniaxial stretch ($\lambda = 1.2$). Plots are reported for each treatment scenario: control (orange), nocodazole (blue) and cytochalasin (green). (a) Comparison between the numerical result (continuous lines) and the experimental data reported in [18] (dashed lines) for the evolution of external radius. The latter is normalised with respect to r_{60} , the radius of the axon at $t = 60$ minutes, immediately after stretch. The shaded regions indicate error bar in standard deviation relatively to the experimental data. (b) Plots of a_{Θ} (continuous lines) and a_Z (dashed lines) averaged over the cortex sectional area. (c) Evolution of radial stress T_{rr} at the interface $r = r_i$, normalised with respect to the shear modulus of the sound cortex.

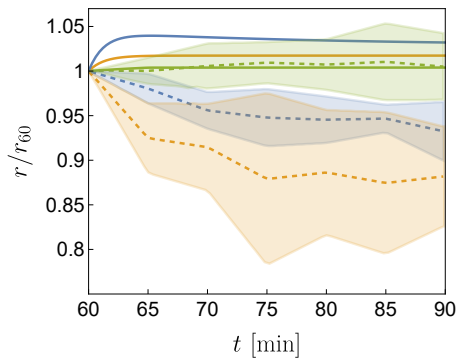


FIGURE 8. Monoparametric approach: plot of the dimensionless radius r/r_{60} (where r_{60} is the radius of the axon at $t = 60$ minutes, immediately after stretch) as a function of time in the case of uniaxial stretch ($\lambda = 1.2$). The numerical results (continuous lines) are compared with the experimental data reported in [18] (dashed lines) for axons treated with nocodazole (blue), cytochalasin (green), and some untreated axons (orange). The shaded regions indicate error bar in standard deviation relatively to the experimental data. The monoparametric approach fails to reproduce the experimental data.

Finally, cytochalasin D is responsible for a disruption of actin filaments in the cortex and the reduction of cortical remodeling stress. As a consequence, both the active stretches a_{Θ} and a_Z undergo a substantial increment which makes them close to 1 after one hour. In this case, the axoplasm behaves as a nearly passive material and the stress is almost completely relaxed (see Fig. 6c).

4.5.2. *Uniaxial stretch.* We first consider the control case, i.e. the stretching of an untreated axon. The radius significantly reduces in time, as shown in Figure 7a. This is the result of cortex remodelling: while a_Z increases to balance the tension due to the axial stretch, a_{Θ} decreases, i.e. the active hoop contraction increases (see Figure 7b). Such a microstructural reorganisation increases axoplasm compression, as shown in Figure 7c. The changes in the axon diameter are amplified by the axoplasm damage, induced by the fast stretch.

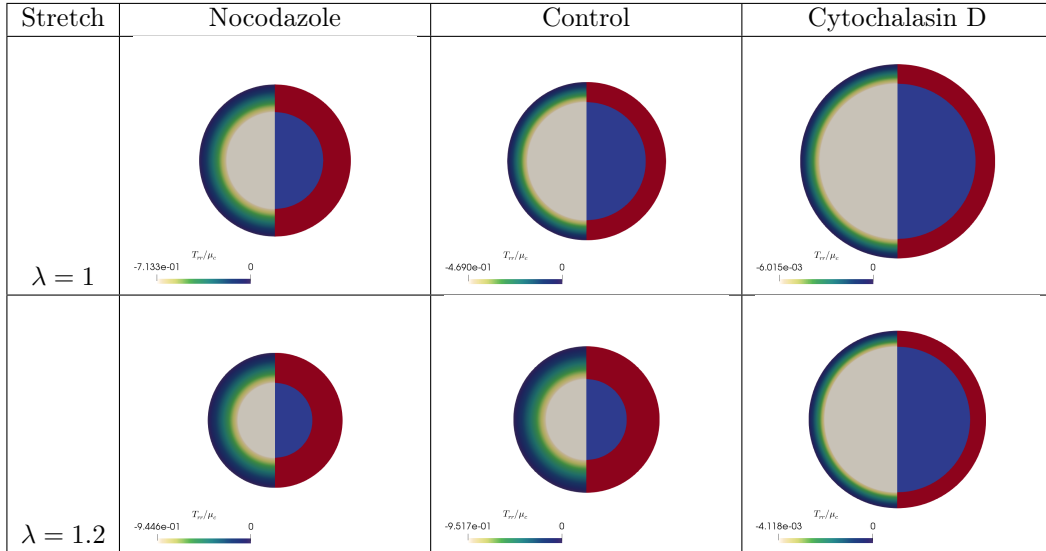


FIGURE 9. Actual transverse section of the axon for $\lambda = 1$ (top) and $\lambda = 1.2$ (bottom) at $t = 60$ min and $t = 90$ min, respectively. In each transverse section, on the left we plot the dimensionless radial stress profile T_{rr}/μ_c , while on the right half we highlight the actual configurations of the axoplasm and of the cortex, represented as the blue and the red areas, respectively.

The dynamics of nocodazole-treated axons under uniaxial stretching is similar, although the induced thinning is less pronounced when compared to the control case. We remark that axons treated with nocodazole are already damaged when stretch is applied. Therefore, less microtubules are depolymerised as a result of the deformation, and the initial state is closer to the final equilibrium state, as depicted in Figure 7b. Instead, the evolution of a_Z is almost the same in both cases. Qualitatively similar trends are also observed in Figure 7c where we plot the radial stress T_{rr} at the interface as a function of time: radius reduction is correlated with an increased compression of the axoplasm.

Finally, we consider the stretching of axons exposed to cytochalasin D. In Figure 7a, we see that the radius is almost constant in time after the deformation. Indeed, as shown in Figure 7b, both the active stretches are close or equal to 1, so that the cortex behaves as nearly passive material. The constant diameter as result of F-actin depolymerisation supports our conjecture. In order to maintain a homeostatic stress state during stretching, the cortex actively reorganise itself and induces changes in the axon diameter.

In Section 3.2, based on the analysis performed in the incompressible case, we argued that imposing *a priori* a linear relation between the circumferential and the axial active stretches is not suitable to reproduce the experimental data in the case of the uniaxially stretched axon. This remains true also under the more realistic hypothesis of a compressible axon. Indeed, in Figure 8, we plot the dynamics of the axonal radius in all the three cases (control, nocodazole and cytochalasin D-treated axons). The derivation of the evolution equation used in this numerical simulation is detailed in A. From Figure 8, we see that the monoparametric model fails to fit the experimental curves and the reasons for that qualitatively rely on the considerations discussed in Section 3.2.

To better visualise how the stress profile affects the shape of the axon, in Figure 9 we show the actual transverse section at the final instant of time. Here, we plot the nondimensionalised radial stress T_{rr}/μ_c . We observe that thinning of axons appears to be correlated with cortex thickening.

5. DISCUSSION AND CONCLUDING REMARKS

In this work, we have proposed a continuum model to predict the active contraction of the axonal cortex when the axon is subjected to chemo-mechanical stimuli.

By modelling the axon as a continuum hyperelastic body, we have used the active strain approach to describe cortex contractility. The active contraction of the cortex is regulated by an extra balance

law motivated by the work of DiCarlo and Quiligotti on growth [16]. In particular, equation (8) describes the equilibrium between the action of external active forces (modeled by B_Θ and B_Z) and the resistance of the material to remodelling, which we have called internal remodelling stresses and labelled as C_Θ and C_Z . We have then obtained thermodynamically consistent constitutive laws by following the Coleman-Noll procedure. We have extended the standard dissipation inequality for elastic bodies under isothermal conditions to account for the power of the cortex active contraction. More specifically, we have obtained the classic constitutive equation for the Piola-Kirchhoff stress tensor and some constitutive restrictions on C_Θ and C_Z . A simple admissible choice for the internal remodelling stresses is provided by (12).

By using such constitutive laws, the remodelling balance law in (8) becomes the system of differential equations in (20). This system regulates the time evolution of the hoop and axial components of the active stretch. Such equations exhibit some key features if compared with models of stress-modulated growth for biological tissues [16, 4]. Indeed, as can be seen in Eq. (20), the system evolves towards a steady state. Specific combinations of the Mandel stress tensor components associated to such equilibrium state are uniform throughout the cortex, namely $\mathbf{M} : \mathbf{l}_j = -B_j$. Thus, the axon reacts to external chemo-mechanical stimuli by regulating the active contraction to target a homeostatic stress state.

We have then assumed the axon to be incompressible. In this context, the evolution equations reduce to the nonlinear dynamical system (36). Through a linear stability analysis, we have proved the existence of a single asymptotically stable solution associated to the above mentioned homeostatic state.

Then, by using a more suitable compressible constitutive model, we have implemented numerical simulations of axon dynamics in FEniCS and validated our numerical results with the experiments reported in [18]. In our simulations we have modelled the equilibrium behaviour of the axon followed by a uni-axial deformation of 20% stretch. We have reproduced three scenarios: a) control case, b) the disruption of F-actin filaments when axons are exposed to cytochalasin D and c) the depolymerisation of microtubules following the application of nocodazole. In our numerical model, the effect of the drugs is accounted for by introducing a damage function that modifies the energy functional, as we have discussed in Section 4.1. Moreover, since in the *in vitro* experiments the axons are pulled at a high strain rate [18], we have assumed that microtubules are further damaged during the axial deformation [43].

The numerical results for all 3 scenarios are in excellent quantitative agreement with the experimental results, as shown in Figures 6-7. Indeed, the diameter progressively increases when F-actin filaments are disrupted, while a decrease of the transverse section area with respect to the control case is observed when microtubules are depolymerised. We have shown that the diameter of axons is regulated by the compressive stress applied on the axoplasm by the cortex. Diameter reduction appears to be correlated with a thickening of the axonal cortex, as shown in Figure 9.

Our results support the hypothesis of a coupled mechanism between the axial and hoop active stretches [18]. The cortex undergoes a microstructural reorganisation to modulate its stress state and regulates axon diameter by compressing the axoplasm. Understanding such mechanism may represent a preliminary step towards a better understanding of the physical causes which underlie axon morphological degeneration as a consequence of neurodegenerative diseases, viral infections, and traumatic strain injuries [13, 36].

Future works will focus on the analysis of such systems that, when subjected to displacements, break their axial symmetry. Furthermore, it would be interesting to study the effect of morphological changes of the axon on its ability to transmit electro-chemical signals.

Authors' contribution. All the authors equally contributed to the study.

Declaration of Competing Interests. The authors declare that they have no known competing financial interests or personal relationships that could have appeared to influence the work reported in this paper.

Acknowledgements. D.A., G.B., G.L., G.P, and D.R. acknowledge support by the National Group of Mathematical Physics (GNFM – INdAM) through the program Progetto Giovani 2020. G.B. and G.L. acknowledge support by Progetto d'Eccellenza 2018 – 2022 funded by Ministero

dell'Università e della Ricerca (code: E11G18000350001). D.R. acknowledges support by Regione Lombardia project NEWMED (ID: 1175999 POR FESR 2014-2020). We thank D. Ambrosi, A. Di Carlo, A. Lucantonio, and G. Noselli for fruitful discussions.

APPENDIX A. MONOPARAMETRIC ACTIVE STRETCH

In the following, we discuss the case of a single active stretch parameter, where the tensor \mathbf{F}_a is given by (44).

In such case, the balance equations (8) for the remodelling stresses reduce to a single equation, namely $B = C$. The Clausius-Duhem (9) inequality reduces to

$$\int_{\mathcal{P}} \dot{\Psi} \, dV \leq \int_{\mathcal{P}} \mathbf{P} : \dot{\mathbf{F}} \, dV + 2 \int_{\mathcal{P} \cap \Omega_{0c}} C \frac{\dot{a}}{a} \, dV.$$

By performing analogous computations to those in Section 2, we find

$$(52) \quad \begin{cases} \mathbf{P} = \frac{\partial \Psi_0}{\partial \mathbf{F}_e} \mathbf{F}_a^{-T}, \\ 2C = \mu_c \tau \frac{\dot{a}}{a} - \mathbf{M} : \hat{\mathbf{I}} + \Gamma, \end{cases}$$

where

$$\hat{\mathbf{I}} = \mathbf{E}_\Theta \otimes \mathbf{E}_\Theta + \mathbf{E}_Z \otimes \mathbf{E}_Z - 2\mathbf{E}_R \otimes \mathbf{E}_R,$$

and Γ is the reactive term that enforce the unilateral constraint $a \leq 1$. Similarly to (20), the evolution equation for the active stretch reads as follows

$$(53) \quad \dot{a} = \begin{cases} \frac{1}{\mu_c \tau} (2B + \mathbf{M} : \hat{\mathbf{I}}) a, & \text{if } a < 1 \text{ or } 2B < -\mathbf{M} : \hat{\mathbf{I}}, \\ 0, & \text{otherwise.} \end{cases}$$

The evolution equation (53) is valid for a compressible constitutive laws and it is used to obtain Figure 8. As done in Section 3, the derivation of the constitutive laws is done by replacing Ψ with Ψ_{ext} , which is defined in (27). In particular, the expression of (53) is also valid in the incompressible case.

A.1. Incompressible case. In the following, we study (53). Similarly to Section 3, the axon is assumed to behave as an incompressible neo-Hookean material. The corresponding strain energy density is (28). By assuming cylindrical symmetry as in (21), the differential equation (53) admits an equilibrium \bar{a} . Indeed, we have an equilibrium solution with $\bar{a} < 1$ if

$$(54) \quad f(a) = 2\mu_c a^6 - 2B\lambda a^2 - \mu_c (\lambda^3 + 1) = 0.$$

Since $f(0) < 0$, $f'(a) > 0$ for $B \leq 0$, and $f(a) \rightarrow +\infty$ as $a \rightarrow +\infty$, there exists one and only one $\bar{a} > 0$ such that $f(\bar{a}) = 0$. Such a root is acceptable if $\bar{a} < 1$, and this holds whenever $f(1) > 0$. It is straightforward to prove the asymptotic stability of \bar{a} . Otherwise, if $f(1) \leq 0$, then $2B + \mathbf{M} : \hat{\mathbf{I}}$ is non-negative for $a = 1$ and the equilibrium solution is $\bar{a} = 1$.

To compute the stress components, we need to explicitly obtain the expression for p . By setting $a_\Theta = a_Z = a$ in (31)-(32), we get

$$\begin{aligned} p(r) &= \hat{k}_1, & 0 \leq r < r_i, \\ p(r) &= \hat{k}_2 + \frac{(a^6 - 1)\mu_c \log(r)}{\lambda a^2}, & r_i \leq r < r_o. \end{aligned}$$

By enforcing the boundary and the interface conditions, (26) and (7) respectively, we find the two constants

$$\hat{k}_1 = \frac{\mu_a}{\lambda} + \frac{\mu_c (a^6 - 1) [\log(r_i) - \log(r_o)]}{\lambda a^2},$$

and

$$\hat{k}_2 = \frac{\mu_c (a^6 + \log(r_o) - a^6 \log(r_o))}{\lambda a^2}.$$

REFERENCES

- [1] GitHub repository containing the numerical code. https://github.com/giupoz/axon_active_regulation.git.
- [2] M. Alnæs, J. Blechta, J. Hake, A. Johansson, B. Kehlet, A. Logg, C. Richardson, J. Ring, M. E. Rognes, and G. N. Wells. The FEniCS project version 1.5. *Archive of Numerical Software*, 3(100), 2015.
- [3] M. S. Alnæs, A. Logg, K. B. Ølgaard, M. E. Rognes, and G. N. Wells. Unified form language: A domain-specific language for weak formulations of partial differential equations. *ACM Transactions on Mathematical Software (TOMS)*, 40(2):1–37, 2014.
- [4] D. Ambrosi and F. Guana. Stress-modulated growth. *Mathematics and Mechanics of Solids*, 12(3):319–342, nov 2005.
- [5] D. Ambrosi and S. Pezzuto. Active stress vs. active strain in mechanobiology: Constitutive issues. *Journal of Elasticity*, 107(2):199–212, jul 2011.
- [6] A. C. Bain and D. F. Meaney. Tissue-level thresholds for axonal damage in an experimental model of central nervous system white matter injury. *Journal of Biomechanical Engineering*, 122(6):615–622, 2000.
- [7] R. Bernal, P. A. Pullarkat, and F. Melo. Mechanical properties of axons. *Physical Review Letters*, 99(1):018301, 2007.
- [8] D. Bray. Axonal growth in response to experimentally applied mechanical tension. *Developmental Biology*, 102(2):379–389, 1984.
- [9] S. Chada, P. Lamoureux, R. E. Buxbaum, and S. R. Heidemann. Cytomechanics of neurite outgrowth from chick brain neurons. *Journal of Cell Science*, 110(10):1179–1186, 1997.
- [10] P. G. Ciarlet. *Mathematical Elasticity: Three-Dimensional Elasticity*. Society for Industrial and Applied Mathematics, Philadelphia, PA, 2021.
- [11] B. D. Coleman and W. Noll. The thermodynamics of elastic materials with heat conduction and viscosity. In *The Foundations of Mechanics and Thermodynamics*, pages 145–156. Springer Berlin Heidelberg, 1974.
- [12] A. R. Costa, S. C. Sousa, R. Pinto-Costa, J. C. Mateus, C. D. Lopes, A. C. Costa, D. Rosa, D. Machado, L. Pajuelo, X. Wang, et al. The membrane periodic skeleton is an actomyosin network that regulates axonal diameter and conduction. *Elife*, 9:e55471, 2020.
- [13] A. Datar, J. Ameeramja, A. Bhat, R. Srivastava, A. Mishra, R. Bernal, J. Prost, A. Callan-Jones, and P. A. Pullarkat. The roles of microtubules and membrane tension in axonal beading, retraction, and atrophy. *Biophysical Journal*, 117(5):880–891, sep 2019.
- [14] M. Dehghany, R. Naghdabadi, S. Sohrabpour, Y. Li, and Y. Hu. A thermodynamically consistent electro-chemo-mechanical theory for modeling axonal swelling. *Journal of the Mechanics and Physics of Solids*, 145:104113, dec 2020.
- [15] T. J. Dennerll, P. Lamoureux, R. E. Buxbaum, and S. R. Heidemann. The cytomechanics of axonal elongation and retraction. *Journal of Cell Biology*, 109(6):3073–3083, dec 1989.
- [16] A. DiCarlo and S. Quiligotti. Growth and balance. *Mechanics Research Communications*, 29(6):449–456, nov 2002.
- [17] M. Epstein. Mathematical characterization and identification of remodeling, growth, aging and morphogenesis. *Journal of the Mechanics and Physics of Solids*, 84:72–84, nov 2015.
- [18] A. Fan, A. Tofangchi, M. Kandel, G. Popescu, and T. Saif. Coupled circumferential and axial tension driven by actin and myosin influences in vivo axon diameter. *Scientific Reports*, 7(1), oct 2017.
- [19] J. A. García-Grajales, A. Jérusalem, and A. Goriely. Continuum mechanical modeling of axonal growth. *Computer Methods in Applied Mechanics and Engineering*, 314:147–163, feb 2017.
- [20] G. Giamtesio, A. Musesti, and D. Riccobelli. A comparison between active strain and active stress in transversely isotropic hyperelastic materials. *Journal of Elasticity*, 137(1):63–82, dec 2018.
- [21] A. Goriely. *The Mathematics and Mechanics of Biological Growth*. Springer New York, 2017.
- [22] M. E. Gurtin, E. Fried, and L. Anand. *The mechanics and thermodynamics of continua*. Cambridge University Press, 2010.
- [23] M. A. Holland, K. E. Miller, and E. Kuhl. Emerging brain morphologies from axonal elongation. *Annals of biomedical engineering*, 43(7):1640–1653, 2015.
- [24] H. Jacomy, G. Fragoso, G. Almazan, W. E. Mushynski, and P. J. Talbot. Human coronavirus OC43 infection induces chronic encephalitis leading to disabilities in BALB/c mice. *Virology*, 349(2):335–346, jun 2006.
- [25] V. Kondaurov and L. Nikitin. Finite strains of viscoelastic muscle tissue. *Journal of Applied Mathematics and Mechanics*, 51(3):346–353, jan 1987.
- [26] G. E. Lang, S. L. Waters, D. Vella, and A. Goriely. Axonal buckling following stretch injury. *Journal of Elasticity*, 129(1):239–256, 2017.
- [27] P. C. Letourneau. Actin in axons: stable scaffolds and dynamic filaments. *Cell Biology of the Axon*, pages 265–290, 2009.
- [28] A. Logg, G. N. Wells, and J. Hake. DOLFIN: A C++/Python finite element library. In *Automated solution of differential equations by the finite element method*, pages 173–225. Springer, 2012.
- [29] J. Mandel. Thermodynamics and plasticity. In J. J. Delgado Domingos, M. N. R. Nina, and J. H. Whitelaw, editors, *Foundations of Continuum Thermodynamics*, chapter 15, pages 283–304. Macmillan Education UK, 1973.
- [30] P. Nardinocchi and L. Teresi. On the active response of soft living tissues. *Journal of Elasticity*, 88(1):27–39, jun 2007.

- [31] I. Nikić, D. Merkler, C. Sorbara, M. Brinkoetter, M. Kreutzfeldt, F. M. Bareyre, W. Brück, D. Bishop, T. Mischel, and M. Kerschensteiner. A reversible form of axon damage in experimental autoimmune encephalomyelitis and multiple sclerosis. *Nature Medicine*, 17(4):495–499, 2011.
- [32] H. Oliveri and A. Goriely. Mathematical models of neuronal growth. *Biomechanics and Modeling in Mechanobiology*, pages 1–30, 2022.
- [33] H. Ouyang, E. Nauman, and R. Shi. Contribution of cytoskeletal elements to the axonal mechanical properties. *Journal of Biological Engineering*, 7(1), sep 2013.
- [34] P. Podio-Guidugli. *Continuum Thermodynamics*. Springer, 2019.
- [35] A. Quarteroni. *Numerical Models for Differential Problems*. Springer Milan, Milano, 2014.
- [36] D. Riccobelli. Active elasticity drives the formation of periodic beading in damaged axons. *Physical Review E*, 104(2), aug 2021.
- [37] D. Riccobelli and D. Ambrosi. Activation of a muscle as a mapping of stress–strain curves. *Extreme Mechanics Letters*, 28:37–42, apr 2019.
- [38] C. Rotsch and M. Radmacher. Drug-induced changes of cytoskeletal structure and mechanics in fibroblasts: An atomic force microscopy study. *Biophysical Journal*, 78(1):520–535, jan 2000.
- [39] J. Stålhand, A. Klarbring, and G. Holzapfel. A mechanochemical 3d continuum model for smooth muscle contraction under finite strains. *Journal of Theoretical Biology*, 268(1):120–130, jan 2011.
- [40] G. B. Stokin, C. Lillo, T. L. Falzone, R. G. Brusch, E. Rockenstein, S. L. Mount, R. Raman, P. Davies, E. Masliah, D. S. Williams, et al. Axonopathy and transport deficits early in the pathogenesis of alzheimer’s disease. *Science*, 2005.
- [41] L. A. Taber and R. Perucchio. Modeling heart development. *Journal of Elasticity and the Physical Science of Solids*, 61(1):165–197, 2000.
- [42] P. Tagliaferro and R. E. Burke. Retrograde axonal degeneration in parkinson disease. *Journal of Parkinson’s disease*, 6(1):1–15, 2016.
- [43] M. D. Tang-Schomer, A. R. Patel, P. W. Baas, and D. H. Smith. Mechanical breaking of microtubules in axons during dynamic stretch injury underlies delayed elasticity, microtubule disassembly, and axon degeneration. *The FASEB Journal*, 24(5):1401–1410, dec 2009.
- [44] C. Truesdell and W. Noll. The Non-Linear Field Theories of Mechanics. *Handbuch der Physik*, 2:1–541, 1965.
- [45] K. Xu, G. Zhong, and X. Zhuang. Actin, spectrin, and associated proteins form a periodic cytoskeletal structure in axons. *Science*, 339(6118):452–456, jan 2013.
- [46] Y. Zhang, K. Abiraman, H. Li, D. M. Pierce, A. V. Tzingounis, and G. Lykotraftitis. Modeling of the axon membrane skeleton structure and implications for its mechanical properties. *PLOS Computational Biology*, 13(2):e1005407, feb 2017.
- [47] J. Zheng, P. Lamoureux, V. Santiago, T. Dennerll, R. E. Buxbaum, and S. R. Heidemann. Tensile regulation of axonal elongation and initiation. *Journal of Neuroscience*, 11(4):1117–1125, 1991.

MOX Technical Reports, last issues

Dipartimento di Matematica
Politecnico di Milano, Via Bonardi 9 - 20133 Milano (Italy)

- 69/2022** Franco, N.R.; Manzoni, A.; Zunino, P.
Learning Operators with Mesh-Informed Neural Networks
- 68/2022** Orlando, G.; Benacchio, T.; Bonaventura, L.
An IMEX-DG solver for atmospheric dynamics simulations with adaptive mesh refinement
- 67/2022** Alghamdi, M. M.; Boffi, D.; Bonizzoni, F.
A greedy MOR method for the tracking of eigensolutions to parametric elliptic PDEs
- 63/2022** Corti, M.; Antonietti, P.F.; Dede', L.; Quarteroni, A.
Numerical Modelling of the Brain Poromechanics by High-Order Discontinuous Galerkin Methods
- 66/2022** Antonietti, P.F.; Liverani, L.; Pata, V.
Lack of superstable trajectories in linear viscoelasticity: A numerical approach
- 65/2022** Dassi, F.; Fumagalli, A.; Mazzieri, I.; Vacca, G.
Mixed Virtual Element approximation of linear acoustic wave equation
- 64/2022** Massi, M.C., Dominoni, L., Ieva, F., Fiorito, G.
A Deep Survival EWAS approach estimating risk profile based on pre-diagnostic DNA methylation: an application to Breast Cancer time to diagnosis
- 62/2022** Ciaramella, G.; Halpern, L.; Mechelli, L.
Convergence analysis and optimization of a Robin Schwarz waveform relaxation method for periodic parabolic optimal control problems
- 61/2022** Gregorio, C.; Cappelletto, C.; Romani, S.; Stolfo, D.; Merlo, M.; Barbati, G.
Using marginal structural joint models to estimate the effect of a time-varying treatment on recurrent events and survival: An application on arrhythmogenic cardiomyopathy
- 59/2022** Boon, W. M.; Fumagalli, A.
A multipoint vorticity mixed finite element method for incompressible Stokes flow